HEAT TRANSFER ASIAN RESEARCH

Online ISSN: 1523-1496

PUBLISHER: WILEY (NEW YORK, USA)

ACCEPTED JUNE 5TH 2017

BIOCONVECTIVE ELECTROMAGNETIC NANOFLUID TRANSPORT FROM A WEDGE GEOMETRY: *SIMULATION OF SMART ELECTRO-CONDUCTIVE BIO-NANO-POLYMER PROCESSING*

***FatemaTuz ZOHRA*[a], *Mohammed Jashim UDDIN* [b], *and Ahmad Izani MD. ISMAIL* [a]**
[a]School of Mathematical Sciences, Universiti Sains Malaysia, 11800, Penang, Malaysia.
[b]Head and Professor of Mathematics Department, American International University-Bangladesh, Kuratoli Road, Dhaka, Bangladesh.
O. Anwar Bég [c]
[c] Fluid Mechanics, Bio-Propulsion and Nano-Systems, Aeronautical and Mechanical Engineering Division, Room G77, Newton Building, University of Salford, M54WT, UK.

[b]Corresponding author: Email:jashim_74@yahoo.com

ABSTRACT

A mathematical model is presented for steady, two-dimensional, stagnation-point flow, heat, mass, and micro-organism transfer in a viscous, incompressible, bioconvective, electromagnetic nanofluid along a wedge with Stefan blowing effects, hydrodynamic slip, and multiple convective boundary conditions. Gyrotactic micro-organisms are present in the nanofluid and bioconvection arises, characterized by micro-organisms swimming under a competing torque. Similarity transformations are used to render the system of governing partial differential equations into a system of coupled similarity equations. The transformed equations are solved numerically with the BVP5C method. The impact of emerging parameters on dimensionless velocity, temperature, magnetic induction function, nanoparticle volume fraction, and density of motile micro-organisms is studied graphically. Furthermore, the responses of the local skin friction, local Nusselt number, local Sherwood number, and the wall gradient of density of motile micro-organism number to variation in these parameters are elaborated. Validation of solutions with previous studies based on special cases of the general model is included. The simulations are relevant to the processing of biological, electro-conductive nanomaterials and industrial hygienic coating systems exploiting combined electromagnetics, nano-systems, and microscopic, bio-propulsion mechanisms.

Keywords: *Bioelectromagnetics; nanofluids; Stefan blowing; bio-nano-materials processing; micro-organism gyrotaxis*

NOMENCLATURE

a velocity slip parameter $\left(\frac{(N_1)_0 \upsilon \sqrt[4]{Re}}{L}\right)(-)$

A reciprocal of magnetic Prandtl number $\left(\frac{\xi}{\upsilon}\right)\left(\frac{sK^4}{W}\right)(-)$

$\tilde{b}$ chemotaxis constant (m)

C nanoparticles volume fraction $(-)$

C_f nanoparticles volume fraction at the free stream $(-)$

C_p specific heat at constant pressure $\left(\frac{J}{Kg\,K}\right)$

C_w nanoparticles volume fraction at the wall $(-)$

C_∞ ambient nanoparticles volume fraction at the wall $(-)$

$C_{f\bar{x}}$ local skin friction coefficient $(-)$

D_B Brownian diffusion coefficient $\left(\frac{m^2}{s}\right)$

D_m micro-organism diffusivity coefficient $\left(\frac{m^2}{s}\right)$

D_n diffusivity coefficient $\left(\frac{m^2}{s}\right)$

D_T thermophoretic diffusion coefficient $\left(\frac{m^2}{s}\right)$

E_0 reference electric potential value $(-)$

E_f electric field coefficient $\left(\frac{E_0 \sigma L^3}{\rho \upsilon^2 Re}\right)\left(\frac{Ws^2}{kg\,K^4}\right)$

$E_{\bar{x}}$ stream-wise electric field strength $(E_0)\left(\frac{kg\,m}{s^3 A}\right)$

$f(\eta)$ dimensionless stream function $(-)$

H_0 uniform vertical magnetic field value at the infinity stream $(-)$

H_1 induced magnetic field component along x- direction $\left(\frac{A}{m}\right)$

H_2 induced magnetic field component along y- direction $\left(\frac{A}{m}\right)$

H_e magnetic field at the boundary layer edge $\left(\frac{A}{m}\right)$

$h(\eta)$ dimensionless induced magnetic field function $(-)$

h_c diffusion convection coefficient $(-)$

h_f convection conduction coefficient $(-)$

h_n micro-organism diffusion convection coefficient $(-)$

K thermal conductivity of the nanofluid $\left(\frac{W}{m \cdot K}\right)$

L characteristic length (m)

Lb Lewis number $\left(\frac{\alpha}{D_n}\right)(-)$

M magnetic field parameter $\left(\frac{\mu_m}{4\pi\rho}\left(\frac{H_0 L}{\upsilon}\right)^2\right)(-)$

m wedge parameter $(-)$

N_1 variable velocity slip factor $\left(\frac{s}{m}\right)$

$(N_1)_0$ constant velocity slip factor $(-)$

Nb Brownian motion parameter $\left(\frac{\tau D_B (C_f - C_\infty)}{\alpha}\right)(-)$

Nc convection conduction parameter $\left(\frac{h_f L}{K\sqrt[4]{Re}}\right)(-)$

Nd diffusion convection parameter $\left(\frac{h_c L}{D_n \sqrt[4]{Re}}\right)(-)$

Nn micro-organism diffusion convection parameter $\left(\frac{h_n L}{D_m \sqrt[4]{Re}}\right)(-)$

Nt thermophoresis parameter $\left(\frac{\tau D_T (T_w - T_\infty)}{\alpha T_\infty}\right)(-)$

$N_{n_{\bar{x}}}$ local density number of motile microorganisms $(-)$

$N_{u_{\bar{x}}}$ localNusselt number $(-)$

n number of motile micro-organisms $(-)$

n_w numberof motile micro-organisms at wall (wedge face) $(-)$

n_∞ ambient number of motile micro-organisms $(-)$

P pressure $\left(\frac{kg}{m s^2}\right)(-)$

Pe Péclet number $\left(\frac{\tilde{b} W_c}{D_n}\right)(-)$

Pr Prandtl number $\left(\frac{\upsilon}{\alpha}\right)(-)$

Re Reynolds number $(-)$

$Re_{\bar{x}}$ local Reynolds number $(-)$

s blowing parameter $\left(\frac{C_f - C_\infty}{1 - C_w}\right)(-)$

Sc Schmidt number $\left(\frac{\upsilon}{D_B}\right)$ $(-)$

$Sh_{\bar{x}}$ local Sherwood number $(-)$

t dimensional time (s)

T nanofluid temperature (K)

T_f dimensional free stream temperature (K)

T_w dimensional surface temperature at the wall, i.e., wedge face (K)

T_∞ dimensional ambient temperature (K)

$\bar{u}, \bar{v}$ dimensional velocity components along the $\bar{x}-$ and $\bar{y}-$axes $\left(\frac{m}{s}\right)$

u, v dimensionless velocity components along the $\bar{x}-$ and $\bar{y}-$axes $(-)$

W_c maximum cell swimming speed $\left(\frac{m}{s}\right)$

$\bar{x}, \bar{y}$ Cartesian coordinates along and normal to the plate (m)

x, y dimensionless coordinates along and normal to the plate $(-)$

Greek symbols

α effective thermal diffusivity $\left(\frac{m^2}{s}\right)$

β wedge apex angle

ξ magnetic diffusivity $\left(\frac{1}{4\sigma\pi}\right)\left(\frac{m^2 K^4}{W}\right)$

η independent similarity variable $\left(\frac{m^2}{s}\right)$

μ dynamic viscosity of the nanofluid $\left(\frac{kg}{m\,s}\right)$

μ_m magnetic permeability $\left(\frac{kg\,m}{s^2 A^2}\right)$

υ kinematic viscosity of the fluid $\left(\frac{m^2}{s}\right)$

ρ fluid density $\left(\frac{kg}{m^3}\right)$

ρ_f density of the base fluid $\left(\frac{kg}{m^3}\right)$

$(\rho c_p)_{nf}$ heat capacitance of the nanofluid $\left(\frac{J}{m^3 K}\right)$

$(\rho c)_f$ heat capacitance of the base fluid $\left(\frac{J}{m^3 K}\right)$

$(\rho c)_p$ heat capacitance of the nanoparticles $\left(\frac{J}{m^3 K}\right)$

λ latent heat transfer of the fluid $\left(\frac{W \cdot s}{kg}\right)$

τ ratioof the effective heat capacity of the nanoparticle to the fluid heat capacity $\left(\frac{(\rho c)_p}{(\rho c)_f}\right)(-)$

σ Stefan-Boltzman constant $\left(\frac{W}{m^2 K^4}\right)$

θ dimensionless temperature $(-)$

φ dimensionless nanoparticle volume fraction $(-)$

χ dimensionless number density of motile microorganisms $(-)$

ψ dimensionless stream function $(-)$

ϕ dimensionless magnetic stream function $(-)$

Subscripts

$(\ )'$ differentiation with respect to η

1. INTRODUCTION

Electrohydrodynamics (EHD) is the study of the dynamics of electrically charged fluids [1]. It involves the motion of ionized particles/molecules as well as their interactions with electric fields and surrounding fluid. EHD applications encompass biological transport [2], desalination [3], ion drag pumps in spacecraft propulsion [4], fuel-emulsion mixing optimization [5], and bio-materials processing [6-7]. The application of EHD to heat transfer and mass transport problems also has applications with certain energy system restrictions that require enhanced heat transfer and mass transport. According to Seyed-Yagoobi [8], the advantages of EHD include: (1) rapid and smart control of enhancement by varying the applied electric field; (2) non-mechanical, simple in design, and lightweight; (3) suitability

for special environments (e.g. space); (4) applications to single and multi-phase flows; (5) minimal power consumption; and (6) low noise. However, Seyed-Yagoobi [8] noted that the implementation of high voltage in these promising industrial applications poses design and economic challenges. Further, the implementation of EHD to heat transfer and fluid dynamics introduces complex interactions of many inter-dependent variables. In recent years, heat transfer enhancement utilizing electric fields has been the subject of active research and efforts have been made to explain the EHD phenomena. EHD heat transfer involves the interactions among electric fields, flow fields, and temperature fields as described by Yabe and Hijikata [9] and Marucho and Campo [10]. Atalik and Sönmezle [11-12] investigated the influence of an electric field on heat transfer properties in a laminar, incompressible, non-isothermal boundary layer gas flow over a wedge. Heat transfer enhancement using electric fields with forced convection in a horizontal channel was addressed by Huang and Lai [13]. Mendes and Dente [14] examined the flow over an aerofoil when a layer of ionized gas and a longitudinal electric field are generated in the boundary layer region.

Bio-electromagneticsis the study of the interaction of electric and magnetic fields with biological systems. Bio-electromagnetic fields are frequently used to diagnose illness.Examples include medical imaging, electrocardiography, electroencephalography, and electrophysiological evaluations. These methodologies are often critical in assisting the healing process via therapeutic interventions for cancer, pain control, bone growth, soft tissue repair, neural recovery, etc [15]. However, precautions are essential since excessive exposure to even weak electromagnetic fields or short-term exposure to high strength fields may result in deep electrical burns, neural shock, etc. Many applications of electromagnetic fields in medical engineering are reviewed in ref. [16].

Nanofluids, a sub-branch of these materials, have higher thermal conductivities and convective heat transfer coefficients compared with conventional base fluids (e.g. air and water). Nanofluids are synthesized by suspending nanoparticles, which may be metallic/non-metallic, in base fluids [17]. The applications of nanofluids are immense and still growing. They include antibacterial systems, cancer therapy, pharmacological administration mechanisms, peristaltic pumps for diabetic treatments, solar cell enhancement, coolants for propulsion and lubrication designs[18-19], Beg and Tripathi in [20], and solar collectors [21]. Both theoretical and experimental studies of nanofluids have been reported. In the context of theoretical investigations, many complex geometric systems have been explored and several different numerical techniques employed. Rana in [22] used a finite element algorithm to investigate nonlinear viscoelastic nanofluid flow from an extending sheet as a simulation of nano-polymeric extrusion. Tripathi et al. [23] used Mathematica software integration routines to compute pumping characteristics for transient peristaltic diffusion of nanofluids in tapered channels. Akbar et al. [24] used Nakamura finite difference and integral methods to investigate cilia-driven propulsion of carbon wall nanotube (CNT)nanofluids in porous media with entropy generation effects. Magnetic nanofluids have also drawn significant interest from engineering sciences in recent years. In such flows, the nanoparticle dynamics may be manipulated with externally applied magnetic fields since magnetite nanofluids are electrically conductive. This allows their implementation in various technologies including drug delivery and aerospace smart materials. A state-of-the art review of heat transfer enhancement with magnetic nanofluids has been given by Vékás [25]. Applications in thermal engineering have been documented more recently by Nkurikiyimfura et al. [26].

Bioconvection is an intriguing biological swimming mechanism resulting from complex interactions between phenomena at different physical scales. The process is driven by the

direction of self-propelled micro-organisms that are denser than the suspension fluid. The swimming of each individual micro-organism is a mesoscale physical phenomenon. Micro-organisms characteristically swim in the upwards direction, causing an unstable, top-heavy density stratification which under certain conditions may result in hydrodynamic instability [27]. Bioconvection has been shown to offer the potential to enhance mass transport and induce mixing, especially in micro-volumes, and improve the stability of nanofluids. Khan et al. [28] and many other researchers have analysed various types of bioconvection flows. Mutuku and Makinde [29] investigated the bioconvection induced by the hydromagnetic flow of nanofluid containing nanoparticles andmotile micro-organisms. Khan and Makinde [30] investigated magnetic nanofluid bioconvection due to gyrotactic microorganisms. Zaimi et al. [31] studied stagnation point flow from a stretchable/shrinkable sheet in a nanofluid with micro-organisms. Very recently, Basir et al. [32] examined multiple slip effects in nanofluid enrobing flow from an extending cylindrical body. Bioconvection is driven by *taxis* which may be photonic (light), magnetic, chemical, gravity, torque, or of other types. It is a different propulsion mechanism from other micro-organism dynamics (such as Taylor flagella micro-organism wavy sheet propulsion) as elaborated by Ali et al. [33] and Sajid et al. [34].

All of the above studies have ignored bio-electromagnetic effectsin nanofluids; a feature that may be of critical importance in the synthesis of various next generation bio-nano-polymers, as elucidated by Pérez-Masiá et al. [35]. Biofilms have also been shown to provide a sustainable protective coating to engineering structures which can mitigate corrosion damage [36-37]. The proper understanding of the mechanisms involved in the manufacturing of such materials requires multi-physical fluid dynamic simulation of electro-magneto-hydrodynamics (involving both electrical and magnetic field effects), nanofluid dynamics, as well as heat and micro-organism mass transfer (bioconvection), simultaneously. In the

present article, the bio-electromagnetic nanofluid flow containing gyrotactic micro-organisms along a wedge configuration with multiple convective boundary conditions is considered. The wedge configuration provides several practical scenarios of interest in biotechnological processing e.g. flat sheet, vertical sheet, etc. An efficient numerical technique, implicit finite difference methodwhich is available in MATLAB, is employed to determine numerical solutions for the dimensionless boundary value problem. Verification of the solutions is achieved with the quasi-linearization method solutions of Rajagopal et al. [38]. The influence of emerging nanoscale, magnetic, geometric, bioconvection, and electrical parameters on the velocity, induced magnetic field, temperature, micro-organism number density, and other associated characteristics is evaluated.

2. MATHEMATICAL BIO-ELECTROMAGNETICNANOFLUID MODEL

We consider a steady, two-dimensional stagnation point flow of viscous, incompressible, electrically conducting, water-based nanofluids containing gyrotactic micro-organisms from a stretching/shrinking wedge (with apex angle, β) with multiple convective boundary conditions. The effect of the induced magnetic field is also considered with the magnetic Reynolds number being sufficiently high. Swimming speed is orders of magnitude greater than the sedimentation speed of the micro-organisms. Thus, sedimentation effects are ignored. The physical flow model and coordinate system is shown in **Fig. 1**.The coordinate system is selected such that the $\bar{x}-$axis is aligned with the wedge face and the $\bar{y}-$axis is perpendicular to it. At the wedge surface,$(\bar{y}=0)$,the temperature, T, nanoparticle volume fraction, C, and micro-organism number density, *n*,are prescribed constant values of T_w, C_w, n_w, respectively. The ambient values (as $\bar{y}\to\infty$), the temperature, nanoparticle volume fraction, and micro-organism number density are T_∞, C_∞, n_∞, respectively.

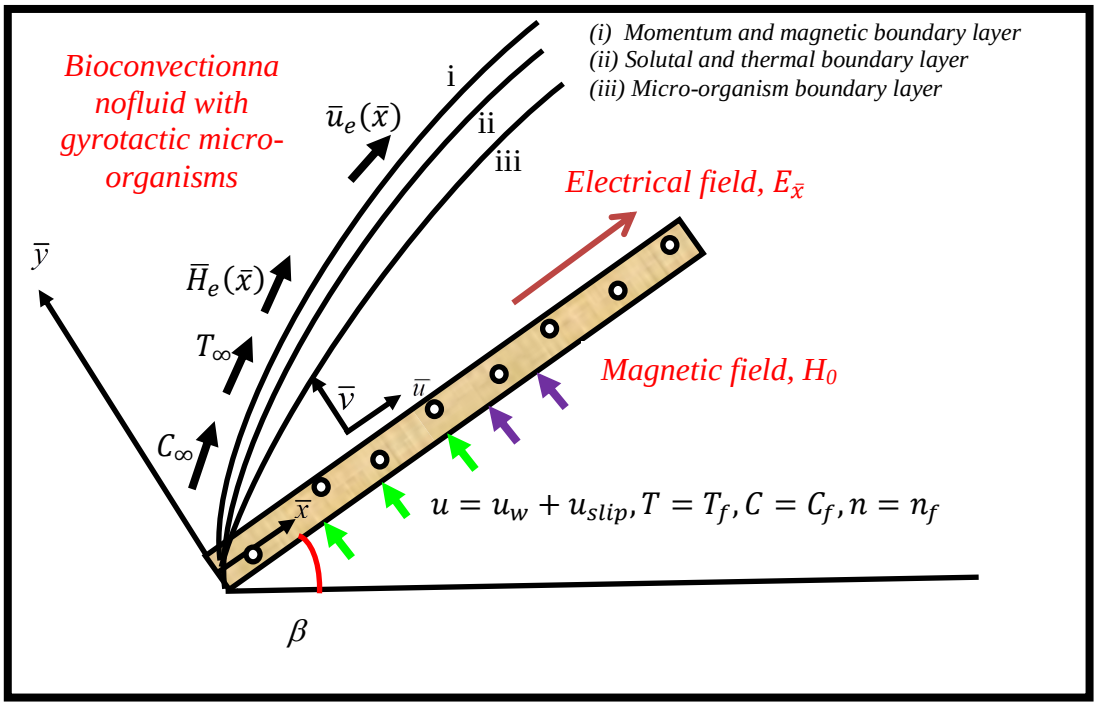

Fig. 1: Physical model and coordinate system for wedge geometry

It is assumed that the velocity of the wedge is $\bar{u}_w = \lambda\sqrt{\mathrm{Re}}\left(\frac{\upsilon}{L}\right)\left(\frac{\bar{x}}{L}\right)^m$, where λ is a constant. It is further assumed that the velocity of the external flow $\bar{u}_e = \sqrt{\mathrm{Re}}\left(\frac{\upsilon}{L}\right)\left(\frac{\bar{x}}{L}\right)^m$, where L is characteristic length and m is the wedge parameter. For the case of $m = 0$, the flow corresponds to that over a flat plate and for $m \neq 0$, the general case of flow over a wedge is taken. A magnetic field of strength H_0 is applied in the direction parallel to the surface of the body (i.e., along the $\bar{x}-$axis outside the boundary layer). The effects of viscous dissipation, Joule heating, and the Hall current are neglected. The electrical currents flowing in the fluid give rise to an induced magnetic field. It is further assumed that the normal component of the induced magnetic field, H_2, vanishes at the wall and the parallel component, H_1, approaches its given value, H_0. Furthermore, an electrical field, $E_{\bar{x}}$, is imposed along the wedge surface in the $\bar{x}-$direction. The governing equations following [39], [40], and [41] may be formulated as follows:

Continuity equation

$$\frac{\partial \bar{u}}{\partial \bar{x}} + \frac{\partial \bar{v}}{\partial \bar{y}} = 0, \tag{1}$$

Magnetic field continuity equation

$$\frac{\partial \bar{H}_1}{\partial \bar{x}} + \frac{\partial \bar{H}_2}{\partial \bar{y}} = 0, \tag{2}$$

Momentum equation

$$\bar{u}\frac{\partial \bar{u}}{\partial \bar{x}} + \bar{v}\frac{\partial \bar{u}}{\partial \bar{y}} - \frac{\mu_m}{4\pi\rho_f}\left(\bar{H}_1\frac{\partial \bar{H}_1}{\partial \bar{x}} + \bar{H}_2\frac{\partial \bar{H}_1}{\partial \bar{y}}\right) = K\left(\bar{u}_e\frac{d\bar{u}_e}{d\bar{x}} - \frac{\mu_m \bar{H}_e}{4\pi\rho_f}\frac{d\bar{H}_e}{d\bar{x}}\right) + \upsilon\frac{\partial^2 \bar{u}}{\partial \bar{y}^2} + \frac{\sigma}{\rho}E_x, \tag{3}$$

Induced magnetic field equation

$$\bar{u}\frac{\partial \bar{H}_1}{\partial \bar{x}} + \bar{v}\frac{\partial \bar{H}_1}{\partial \bar{y}} - \bar{H}_1\frac{\partial \bar{u}}{\partial \bar{x}} - \bar{H}_2\frac{\partial \bar{u}}{\partial \bar{y}} = A\frac{\partial^2 \bar{H}_1}{\partial \bar{y}^2}, \tag{4}$$

Energy equation

$$\bar{u}\frac{\partial T}{\partial \bar{x}} + \bar{v}\frac{\partial T}{\partial \bar{y}} = \alpha\frac{\partial^2 T}{\partial \bar{y}^2} + \tau D_B\frac{\partial T}{\partial \bar{y}}\frac{\partial C}{\partial \bar{y}} + \tau\left(\frac{D_T}{T_\infty}\right)\left(\frac{\partial T}{\partial \bar{y}}\right)^2, \tag{5}$$

Nanoparticle concentration equation

$$\bar{u}\frac{\partial C}{\partial \bar{x}} + \bar{v}\frac{\partial C}{\partial \bar{y}} = D_B\frac{\partial^2 C}{\partial \bar{y}^2} + \left(\frac{D_T}{T_\infty}\right)\frac{\partial^2 T}{\partial \bar{y}^2}, \tag{6}$$

Micro-organismspecies number density equation

$$\bar{u}\frac{\partial n}{\partial \bar{x}} + \bar{v}\frac{\partial n}{\partial \bar{y}} + \frac{\partial}{\partial \bar{y}}\left(n\tilde{v}\right) = D_n\frac{\partial^2 n}{\partial \bar{y}^2}. \tag{7}$$

The boundary conditions follow [42] and [43] such that:

$$\bar{u}=\bar{u}_w+\bar{u}_{\text{slip}},\quad \bar{v}=-\frac{D_B}{1-C_w}\left(\frac{\partial C}{\partial \bar{y}}\right),\quad \bar{H}_2=0,\quad \frac{\partial \bar{H}_1}{\partial \bar{y}}=0,\quad -k\frac{\partial T}{\partial \bar{y}}=h_f\left(T_f-T_w\right),$$
$$-D_n\frac{\partial C}{\partial \bar{y}}=h_c\left(C_f-C_w\right),\quad -D_m\frac{\partial n}{\partial \bar{y}}=h_n\left(n_f-n_w\right)\quad \text{at}\quad \bar{y}=0,$$
$$\bar{u}=K\bar{u}_e\left(\bar{x}\right)\to K\sqrt{\text{Re}}\left(\frac{\nu}{L}\right)\left(\frac{\bar{x}}{L}\right)^m,\quad \bar{H}_1=K\bar{H}_e\left(\bar{x}\right)\to K\bar{H}_0\sqrt{\text{Re}}\left(\frac{\bar{x}}{L}\right)^m,\tag{8}$$
$$T\to T_\infty,\quad C\to C_\infty,\quad n\to 0\quad \text{as}\quad \bar{y}\to\infty,$$

where $\tau=\dfrac{(\rho c)_p}{(\rho c)_f}$ is the ratio of nanoparticle heat capacity to the base fluid heat capacity, α is the thermal diffusivity, $\xi=\dfrac{1}{4\pi\sigma}$ is the magnetic diffusivity, $A=\dfrac{\xi}{\upsilon}$ is the reciprocal of the magnetic Prandtl number $\tilde{\nu}=\dfrac{\tilde{b}W_c}{\Delta C}\dfrac{\partial C}{\partial \bar{y}}$, ρ_f is the density of the fluid, μ_m is the magnetic permeability, D_B is the Brownian diffusion coefficient, D_T is the thermophoretic diffusion, $\bar{H}_0$ is the value of the uniform magnetic field upstream at infinity, $\bar{u}_e\left(\bar{x}\right)$ and $\bar{H}_e\left(\bar{x}\right)$ are the $\bar{x}-$velocity and $\bar{x}-$magnetic field at the edge of the boundary layer. $\bar{u}_{\text{slip}}=\upsilon N_1\left(\bar{x}/L\right)\dfrac{\partial \bar{u}}{\partial \bar{y}}$, where $N_1\left(\bar{x}/L\right)$ is the slip factor and $E_{\bar{x}}=E_0\left(\dfrac{\bar{x}}{L}\right)^{2m-1}$ is the stream-wise electric field strength.

3. NON-DIMENSIONALIZATION OF THE GOVERNING EQUATIONS

The following dimensionless variables (defined in the nomenclature) are introduced to transform Eqns. (1)-(8) into dimensionless form.

$$x=\frac{\bar{x}}{L},\quad y=\frac{\bar{y}\sqrt[4]{\text{Re}}}{L},\quad u=\frac{\bar{u}\,L}{\nu\sqrt{\text{Re}}},\quad u_e=\frac{\bar{u}_e\,L}{\upsilon\sqrt{\text{Re}}},\ v=\frac{\bar{v}\,L}{\upsilon\sqrt[4]{\text{Re}}},\quad \theta=\frac{T-T_\infty}{T_f-T_\infty},$$
$$\phi=\frac{C-C_\infty}{C_f-C_\infty},\ \chi=\frac{n}{n_w},H_1=\frac{\bar{H}_1}{H_0\sqrt{\text{Re}}},\ H_e=\frac{\bar{H}_e}{H_0\sqrt{\text{Re}}},H_2=\frac{\bar{H}_2}{H_0\sqrt[4]{\text{Re}}}\tag{9}$$

We introduced the momentum stream function, ψ, defined by $u = \frac{\partial \psi}{\partial y}$, $v = -\frac{\partial \psi}{\partial x}$ and the magnetic stream function, Φ, defined by $H_1 = \frac{\partial \Phi}{\partial y}$, $H_2 = -\frac{\partial \Phi}{\partial x}$, and substitute them into Eqns. (3)-(8). This yields the following:

$$\frac{\partial \psi}{\partial y}\frac{\partial^2 \psi}{\partial x \partial y} - \frac{\partial \psi}{\partial x}\frac{\partial^2 \psi}{\partial y^2} - M\left(\frac{\partial \Phi}{\partial y}\frac{\partial^2 \Phi}{\partial x \partial y} - \frac{\partial \Phi}{\partial x}\frac{\partial^2 \Phi}{\partial y^2}\right) - Ku_e\frac{du_e}{dx} + KM\left(H_e\frac{dH_e}{dx}\right) - \frac{\partial^3 \psi}{\partial y^3} - \frac{\sigma L^3}{\rho \upsilon^2 \,\mathrm{Re}}E_x = 0, \tag{10}$$

$$\frac{\partial \psi}{\partial y}\frac{\partial^2 \Phi}{\partial x \partial y} - \frac{\partial \psi}{\partial x}\frac{\partial^2 \Phi}{\partial y^2} - \frac{\partial \Phi}{\partial y}\frac{\partial^2 \psi}{\partial x \partial y} + \frac{\partial \Phi}{\partial x}\frac{\partial^2 \psi}{\partial y^2} - A\frac{\partial^3 \Phi}{\partial y^3} = 0, \tag{11}$$

$$\frac{\partial \psi}{\partial y}\frac{\partial \theta}{\partial x} - \frac{\partial \psi}{\partial x}\frac{\partial \theta}{\partial y} - \frac{1}{\mathrm{Pr}}\frac{\partial^2 \theta}{\partial y^2} - \frac{Nb}{\mathrm{Pr}}\frac{\partial \theta}{\partial y}\frac{\partial \phi}{\partial y} - \frac{Nt}{\mathrm{Pr}}\left(\frac{\partial \theta}{\partial y}\right)^2 = 0, \tag{12}$$

$$\frac{\partial \psi}{\partial y}\frac{\partial \phi}{\partial x} - \frac{\partial \psi}{\partial x}\frac{\partial \phi}{\partial y} - \frac{1}{Sc}\frac{\partial^2 \phi}{\partial y^2} - \frac{1}{Sc}\frac{Nt}{Nb}\frac{\partial^2 \theta}{\partial y^2} = 0, \tag{13}$$

$$\left[\frac{\partial \psi}{\partial y}\frac{\partial \chi}{\partial x} - \frac{\partial \psi}{\partial x}\frac{\partial \chi}{\partial y}\right] + \frac{Pe}{Lb}\frac{\partial}{\partial y}\left[\chi\frac{\partial \phi}{\partial y}\right] - \frac{1}{Lb}\frac{\partial^2 \chi}{\partial y^2} = 0. \tag{14}$$

The boundary conditions reduce from Eqn.(8) to:

$$\begin{aligned} &\frac{\partial \psi}{\partial y} = \lambda x^m + N_1(x)\frac{\sqrt[4]{\mathrm{Re}}}{L}\frac{\partial^2 \psi}{\partial y^2},\ \frac{\partial \psi}{\partial x} = \frac{s}{Sc}\frac{\partial \phi}{\partial y},\ \frac{\partial \Phi}{\partial x} = 0, \frac{\partial^2 \Phi}{\partial y^2} = 0,\ \frac{\partial \theta}{\partial y} = -h_f\frac{L}{K\sqrt[4]{\mathrm{Re}}}(1-\theta), \\ &\frac{\partial \phi}{\partial y} = -h_c\frac{L}{D_n\sqrt[4]{\mathrm{Re}}}(1-\phi)\ \textit{and}\quad \frac{\partial \chi}{\partial y} = -h_n\frac{L}{D_m\sqrt[4]{\mathrm{Re}}}(1-\chi)\ \text{at}\ y = 0 \\ &\frac{\partial \psi}{\partial y} = Kx^m,\ \frac{\partial \Phi}{\partial y} = Kx^m,\ \theta \to 0,\ \phi \to 0,\ \chi \to 0\ \text{as}\ y \to \infty. \end{aligned} \tag{15}$$

The following coordinate transformations are developed using Lie group analysis:

$$\eta = x^{\frac{m-1}{2}}y,\ \psi = x^{\frac{m+1}{2}}f(\eta),\ \Phi = x^{\frac{m+1}{2}}h(\eta), \theta = \theta(\eta),\ \phi = \phi(\eta) \tag{16}$$

Here η is the independent similarity variable and $f(\eta),\ \ h(\eta),\ \ \theta(\eta),\ \ \phi(\eta)$ are dependent similarity variables. Implementing the similarity transformations of Eqn. (14) into Eqns. (9)-(12), the following ordinary differential equations emerge:

$$f'''+\frac{m+1}{2}\left[f\,f''-M\,hh'\right]+m\left(K-f'^{2}\right)-mM\left(K-h'^{2}\right)+E_f=0, \tag{17}$$

$$Ah'''+\frac{m+1}{2}\left(f\,h''-f''h\right)=0, \tag{18}$$

$$\theta''+\Pr\left(\frac{m+1}{2}\right)f\,\theta'+Nb\,\theta'\phi'+Nt\,\theta'^{2}=0, \tag{19}$$

$$\phi''+Sc\left(\frac{m+1}{2}\right)f\,\phi'+\frac{Nt}{Nb}\theta''=0, \tag{20}$$

$$\chi''-Pe\left(\phi'\chi'+\chi\phi''\right)+Lb\left(\frac{m+1}{2}\right)f\,\chi'=0. \tag{21}$$

The boundary conditions now become the following:

$$\begin{aligned}&f'(0)=\lambda+a\,f''(0),\quad f(0)=\frac{2s}{(m+1)Sc}\phi'(0),\quad h(0)=h''(0)=0,\quad \theta'(0)=-Nc\left(1-\theta(0)\right),\\&\phi'(0)=-Nd\left(1-\phi(0)\right),\quad \chi'(0)=-Nn\left(1-\chi(0)\right)\\&f'(+\infty)-K=h'(+\infty)-K=\theta(+\infty)=\phi(+\infty)=\chi(+\infty)=0.\end{aligned} \tag{22}$$

The dimensionless parameter in Eqns.(17)-(22) are defined as $\Pr=\frac{\upsilon}{\alpha}$ (Prandtl number), $Pe=\frac{\tilde{b}W_c}{D_n}$ (Peclet number), $Lb=\frac{\alpha}{D_n}$ (Lewis number), $M=\frac{\mu_m {H_0}^2 L^2}{4\pi\,\rho\upsilon^2}$ (magnetic body force), $Nb=\frac{\tau D_B \Delta C}{\alpha}$ (Brownian motion), $Nt=\frac{\tau D_T\left(T_w-T_\infty\right)}{\alpha T_\infty}$ (thermophoresis), $Sc=\frac{\upsilon}{D_B}$ (Schmidt number), $s=\frac{C_f-C_\infty}{1-C_w}$ (blowing), $a=\frac{\left(N_1\right)_0\upsilon\sqrt[4]{\mathrm{Re}}}{L}$ (velocity slip), $N_1(x)=\left(N_1\right)_0 x^{\frac{1-m}{2}}$ (slip factor), $E=E_0\frac{\sigma L^3}{\rho\upsilon^2\,\mathrm{Re}}$ (electric field coefficient), E_0 reference electric potential value),

$Nn = h_n \dfrac{L}{D_m \sqrt[4]{Re}}$ (microorganism diffusion convection), $Nd = h_c \dfrac{L}{D_n \sqrt[4]{Re}}$ (diffusion convection), and $Nc = h_f \dfrac{L}{K \sqrt[4]{Re}}$ (convection conduction).

4. ENGINEERING DESIGN QUANTITIES

The quantities of interest in the present bio-electro-magnetic nanofluid boundary layer flow problem are the skin friction coefficient, $C_{f\bar{x}}$, the local Nusselt number, $Nu_{\bar{x}}$, the local Sherwood number, $Sh_{\bar{x}}$, and the density number of motile micro-organisms, $Nn_{\bar{x}}$. These are defined individually as:

$$C_{f\bar{x}} = \frac{\mu}{\rho \bar{u}_e^2}\left(\frac{\partial \bar{u}}{\partial \bar{y}}\right)_{\bar{y}=0}, \quad Nu_{\bar{x}} = \frac{-\bar{x}}{T_f - T_\infty}\left(\frac{\partial T}{\partial \bar{y}}\right)_{\bar{y}=0}, Sh_{\bar{x}} = \frac{-\bar{x}}{C_f - C_\infty}\left(\frac{\partial C}{\partial \bar{y}}\right)_{\bar{y}=0}, \quad Nn_{\bar{x}} = \frac{-\bar{x}}{n_w}\left(\frac{\partial n}{\partial \bar{y}}\right)_{\bar{y}=0}. \tag{23}$$

By using the appropriate non-dimensionless variables in Eqn.(9) and Eqn.(23), we obtain

$$\mathrm{Re}_{\bar{x}}^{1/2} C_{f_{\bar{x}}} = f''(0), \ \mathrm{Re}_{\bar{x}}^{-1/2} Nu_{\bar{x}} = -\theta'(0), \ \mathrm{Re}_{\bar{x}}^{-1/2} Sh_{\bar{x}} = -\phi'(0), \mathrm{Re}_{\bar{x}}^{-1/2} Nn_{\bar{x}} = -\chi'(0) \tag{24}$$

where $\mathrm{Re}_{\bar{x}} = \bar{u}_e \, \bar{x} / \upsilon$ is the local Reynolds number.

5. NUMERICAL RESULTS, VALIDATION, AND DISCUSSION

The transport problem amounts to a 12th order system of nonlinear, multi-degree, ordinary differential equations defined by Eqns. (17)–(21) with boundary conditions in Eqn. (22). This boundary value problem is solved computationally using the **BVP5C** code in MATLAB.**BVP5C** is a finite difference computational code, three-stage LobattoIIIA formula. This is a collocation scheme that provides a continuous solution that is uniformly fifth-order accurate. Features such as mesh selection and error control are included in the code. Further details are provided in[44].

Validation of this present numerical method has been conducted with existing solutions in the literature. In the absence of electric field parameter $(E_f = 0)$, magnetic field parameter $(M = 0)$, and latent heat transfer of the fluid $(\lambda = 0)$, thermal conductivity $(K = 1)$, and no slip boundary condition $(a = 0)$, the mathematical model defined by Eqns. (17)–(21) with boundary conditions of Eqn. (22) reduces to the case considered by Jafar et al. [45]. **Table1**shows the comparison for the value of the skin friction function, $f''(0)$, with the published Keller box implicit finite difference results of Jafar et al. [45]. Further validation with the earlier quasi-linearization numerical solutions is also included in **Table 1**. An excellent agreement is found between the present BVP5C computations and the other two solutions. The graphs are drawn for the numerical outcomes and observations are detailed over the effects of the governing parameters on momentum and thermal boundary layers.

Figures 2-8 illustrate selected distributions of the key variables i.e. dimensionless velocity, induced magnetic field, temperature, nano-particle volume fraction, and the micro-organism concentration function with transverse coordinate (η). **Figure 9** displays plots for skin friction coefficient, local Nusselt number, local Sherwood number, and local micro-organism transfer rate respectively. These physical quantities must asymptotically approach zero, i.e. $f'(\eta) - K \to 0, h'(\eta) - K \to 0, \theta(\eta) \to 0, \varphi(\eta) \to 0, \chi(\eta) \to 0$ as $\eta \to \infty$ (for $K = 1$), which are satisfied by all $f'(\eta), h'(\eta), \theta(\eta), \varphi(\eta)$ and $\chi(\eta)$.Inspection of **Figs.2-8** verifies that smooth convergence of profiles in the free stream is achieved and thus an adequately large infinity boundary condition is imposed in the BVP5C code.

Table1: Comparison of the value of the friction factor$f''(0)$when $M = 0,\ \lambda = 0, K = 1, E_f = 0, a = 0$.

$\beta = m$	Rajagopal et *al. [38]* [Quasilinearization Method]	Jafar *et al.* [45] [Keller Box Method]	Present [BVP5C method]
1	1.231289	1.2326	1.232587662

5.1 Effects of the magnetic field parameter, *M*

Figures 2(a)-(c) show the effect of the magnetic field strength on the dimensionless temperature, nanoparticle volume fraction, and motile micro-organismsnumber density.

Figures 2(a) and (c) exhibit the dimensionless temperature and micro-organism increasing with increase of magnetic field parameter and **Fig.2(b)** shows that the dimensionless nanoparticle volume fraction decreases with the increase of the magnetic field parameter.

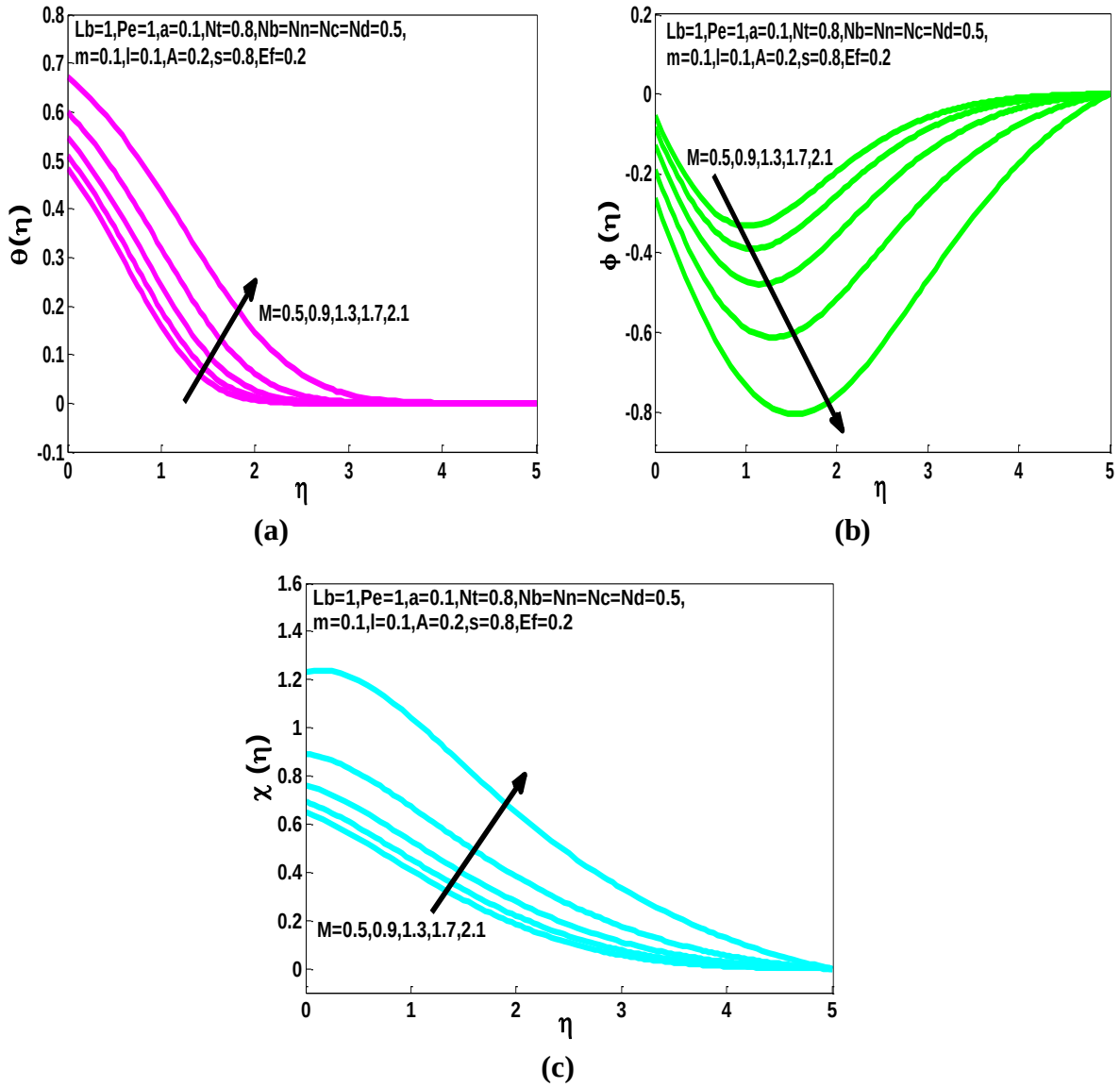

Fig.2: Effect of magnetic field parameter ***M*** on the dimensionless (a) temperature, (b) nanoparticles volume fraction, and (c) motile micro-organisms number density.

Magnetic field parameter, $M = \frac{\mu_m {H_0}^2 L^2}{4\pi \rho \upsilon^2}$ arises in several terms solely in the momentum conservation equation (hydrodynamic boundary layer Eqn. (17)). These terms are $-\left(\frac{m+1}{2}\right)hh^{//}$ and $-mM\left(K - h^{/2}\right)$. Both terms strongly couple the velocity field to the magnetic induction field i.e. Eqn. (18). However, magnetic terms do not appear in the energy conservation (Eqn. (19)), nanoparticle conservation (Eqn. (20)) or micro-organism species (Eqn. (21)) equations. The influence of the magnetic parameter is therefore indirectly sustained via the velocity field which is also coupled strongly to energy, nanoparticle, and micro-organism equations via multiple nonlinear terms in Eqns. (19)-(21). The primary influence of increasing the magnetic parameter is to decelerate the velocity field since the applied magnetic field is transverse to the wedge face, reducing momentum transfer in the boundary layer. However, magnetic induction is elevated by increasing the magnetic parameter. There is effectively a boost in thermal energy in the regime owing to the supplementary kinetic energy dissipated by dragging the nanofluid against the action of the magnetic field. This elevates the temperature magnitudes as illustrated in **Fig.2(a)** and increases thermal boundary layer thickness. The deceleration in the flow with greater magnetic parameter, however, inhibits nanoparticle diffusion (**Fig.2(b)**) and decreases nanoparticle concentration boundary layer thickness. Furthermore, the micro-organism field (**Fig.2(c)**) is positively affected by the damping of the velocity field with greater magnetic force number and is found to grow significantly in magnitude both at and for some distance from the wedge face. Propulsion of the gyrotactic micro-organisms is therefore encouraged with stronger magnetic field effect while nanoparticle volume fraction is reduced. The magnetic field has a profound influence on transport phenomena characteristics.

5.2 Effects of the electric field, E_f

Figures 3(a-e) show the effects of electric field parameter on the dimensionless velocity, induced magnetic field (gradient of the magnetic stream function), temperature, nanoparticle volume fraction, and motile micro-organism number density, respectively.In these figures, the blowing parameter s = 0.8, which assists the flow. The electric body force arising in the momentum Eqn. (17) acts as an *acceleration force* in the flow direction and thereby increases the velocity of the nanofluid. It generates the opposite effect to a magnetic field since the electric field is parallel to the wedge face while the magnetic field is transverse to it. This results in a thinning of the boundary layer and faster growth from the leading edge at the apex angle to downstream locations. The electric field augments magnetic induction, elevating $h'(\eta)$magnitudes. The magnetic boundary layer thickness is also increased. These trends concur with the observations of other researchers including [46] and, more recently,[47]. Increasing electric field, however, generates a cooling effect in the nanofluid and strongly suppresses temperatures, as observed in **Fig.3(c)**. This will lead to an escalation in heat transfer to the wedge face (greater Nusselt numbers). This concurs with the findings of [12]. Thermal boundary layer thickness is also considerably decreased with greater electrical body force. The presence of a stronger aligned axial field is opposite of the transverse magnetic field, which heats the boundary layer. Thus, judicious selection of electric and magnetic fields is required to produce desired thermal effects in the manufacturing of electro-conductive nanofluids. Converse to the impacts of the transverse magnetic field, an increase in aligned electricfield is found to enhance nanoparticle diffusion, i.e. volume fraction magnitudes (**Fig.3(d)**).

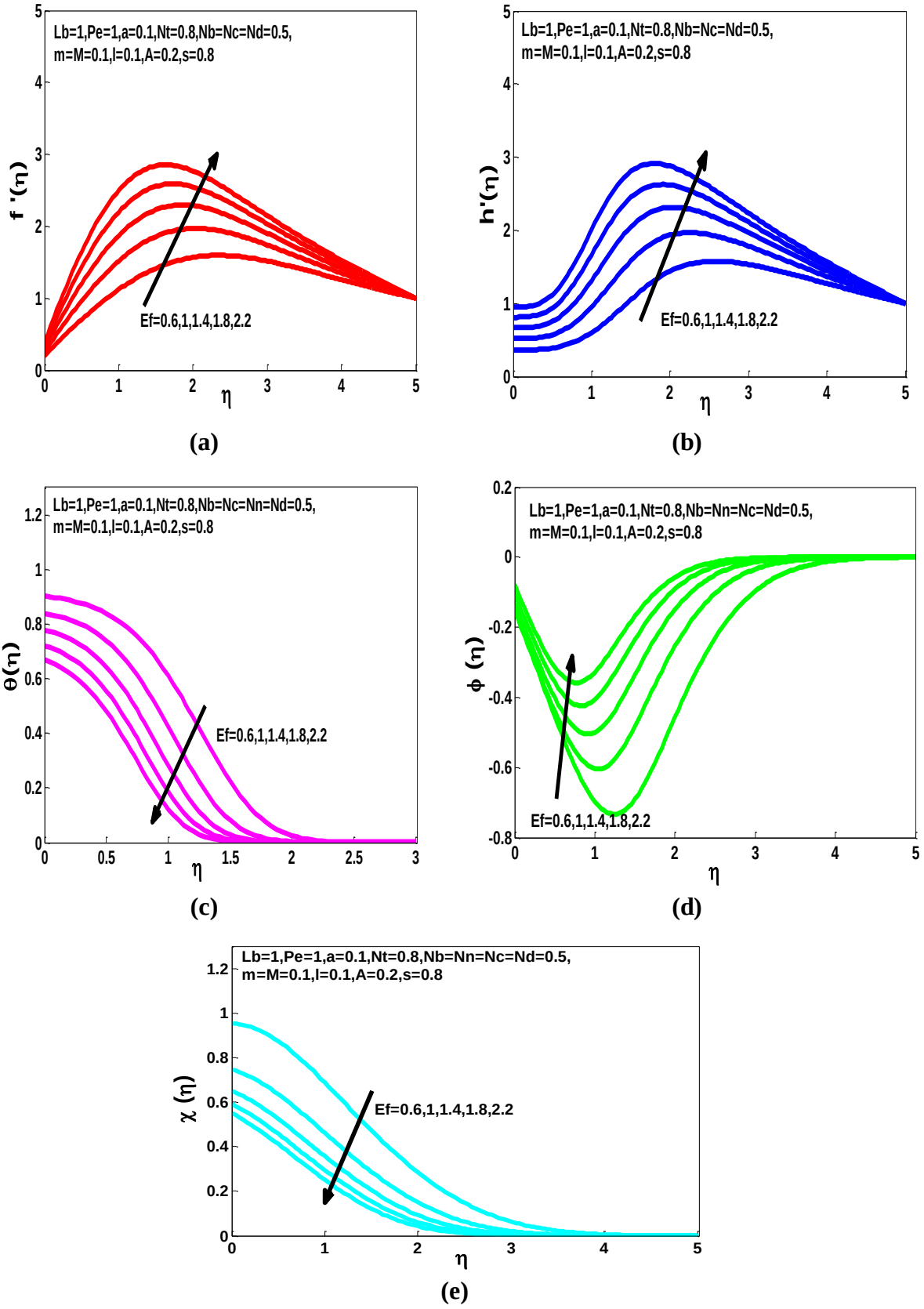

Fig.3: Effects of the electric parameter E_f on the dimensionless (a) velocity, (b) induced magnetic filed , (c) temperature, (d) nanoparticle volume fraction and (e) micro-organism.

This pattern is sustained through the boundary layer transverse to the wedge face i.e. for all values of η. It is also seen that micro-organism density number isinhibited with stronger electric field (**Fig.3(e)**).

5.3 Effects of the convection-conduction parameter, Nc

Figsures 4(a-b) illustrate the impacts of convection-conduction parameter on the dimensionless temperature and nanoparticle volume fraction distributions.

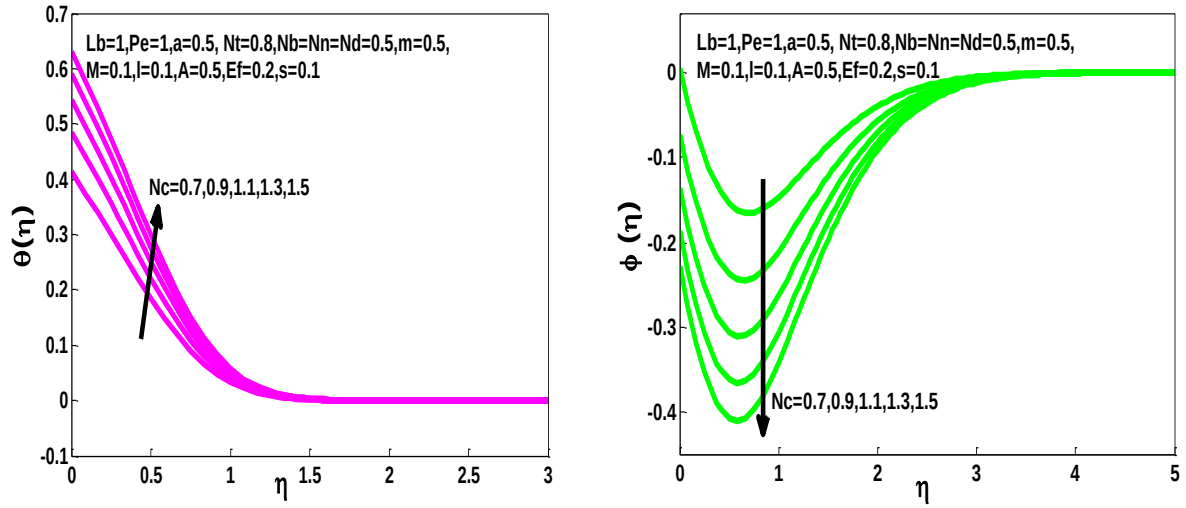

(a) **(b)**

Fig.4: Effects of the convection-conduction parameter ***Nc*** on the dimensionless (a) temperature and (b) nanoparticle volume fraction.

The dimensionless temperature increases and the dimensionless nanoparticle volume fraction decreaseswith an elevation in convection-conduction parameter**.** $Nc = h_f \dfrac{L}{K\sqrt[4]{Re}}$ arises only in the wall temperature boundary condition in Eqn. (22) i.e. at the wedge surface. As Nc increases, thermal convection dominates over thermal conduction in that heat is lost from the wedge surface to the nanofluid, increasing temperatures within the nanofluid. Thermal boundary layer thickness is thereby increased. The increase in thermal diffusion in the nanofluid counteracts species diffusion of nanoparticles and results in a decrease in nanoparticle volume fraction and an associated depletion in nanoparticle concentration

boundary layer thickness. The influence on micro-organism distribution is trivial and is not illustrated. The present computations agree with other investigations such as those reported by [30].

5.4 Effects of the diffusion-convection parameter, *Nd*

Figure 5depicts the response of nanoparticle volume fraction to variation in the diffusion-convection parameter, $Nd = h_c \frac{L}{D_n \sqrt[4]{Re}}$ .This parameter embodies the relative influence of convective diffusion to nanoparticle species diffusivity, and is enforced again at the wedge face via the augmented boundary condition given in Eqn. (22).

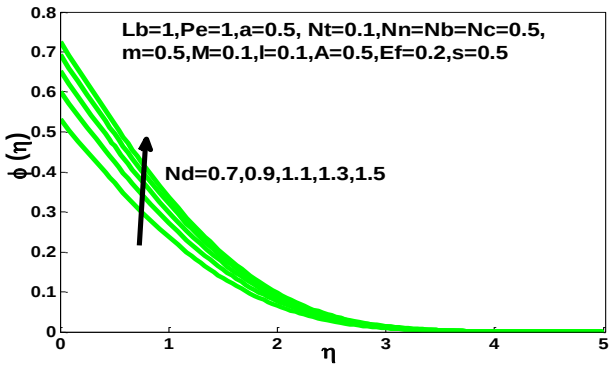

Fig.5: Effects of the diffusion-convection parameter (Nd) on the dimensionless nanoparticles volume fraction.

The most prominent effect is, as expected, at the wall (wedge face). Further into the boundary layer, the influence of *Nd* is progressively reduced and vanishes in the free stream where all nanoparticle volume fractions merge.

5.5 Effects of the micro-organism diffusion-convection parameter, *Nn*

Figure 6shows that a substantial increase in motile micro-organism density number accompanies a rise in micro-organism diffusion-convection parameter. As in other plots,

strong nanofluid injection is present at the wedge face $(s>0)$. The parameter $Nn = h_n \frac{L}{D_m \sqrt[4]{Re}}$ is present in the micro-organism surface boundary condition in Eqn. (22). It relates the comparative contribution of the micro-organism diffusion coefficient at the wall (h_n) to the micro-organism species diffusivity in the nanofluid (D_m). As such, it induces a strong enhancement at the wedge face which is systematically reduced with progression into the boundary layer.

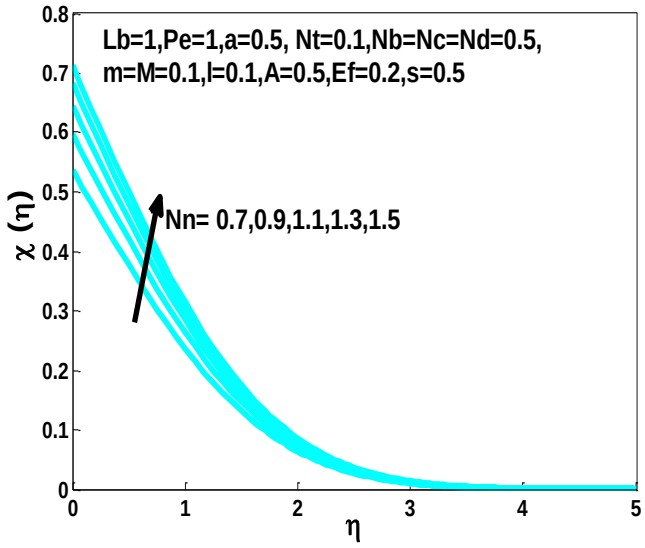

Fig.6: Effects of the micro-organism diffusion-convection parameter ***Nn*** on the dimensionless micro-organism.

5.6 Effects of the suction/blowing parameter, *s*

Figures 7(a-c) depict the influence of the wedge surface suction/blowing parameter, *s* (i.e. lateral mass flux effect) on the dimensionless temperature, nanoparticle volume fraction, and micro-organism number density. **Figures 7(a)** and **7(c)** clearly demonstrate that both dimensionless temperature and micro-organism density are increasedwith greater blowing $(s\rangle 0)$, whereas they are suppressed in magnitude with greater suction $(s\langle 0)$. Conversely,**Fig.7(b)** reveals that nanoparticle volume fraction is decreasedwith an increase in

blowing parameter but enhanced with greater suction. With suction at the wall $(s\langle 0)$, nanofluid is drawn through the wall via perforations. This destroys momentum, increases adherence of the boundary layer to the wall, thereby declerating the flow,leading to a reduction in momentum (hydrodynamic) boundary layer thickness. With greater injection at the wall $(s\rangle 0)$, the opposite effect is generated with a significant accleration of the flow and thinning in the velocity boundary layer thickness. This manifests in a decreasein temperature with stronger suction and an elevation in temperature with stronger injection (blowing).

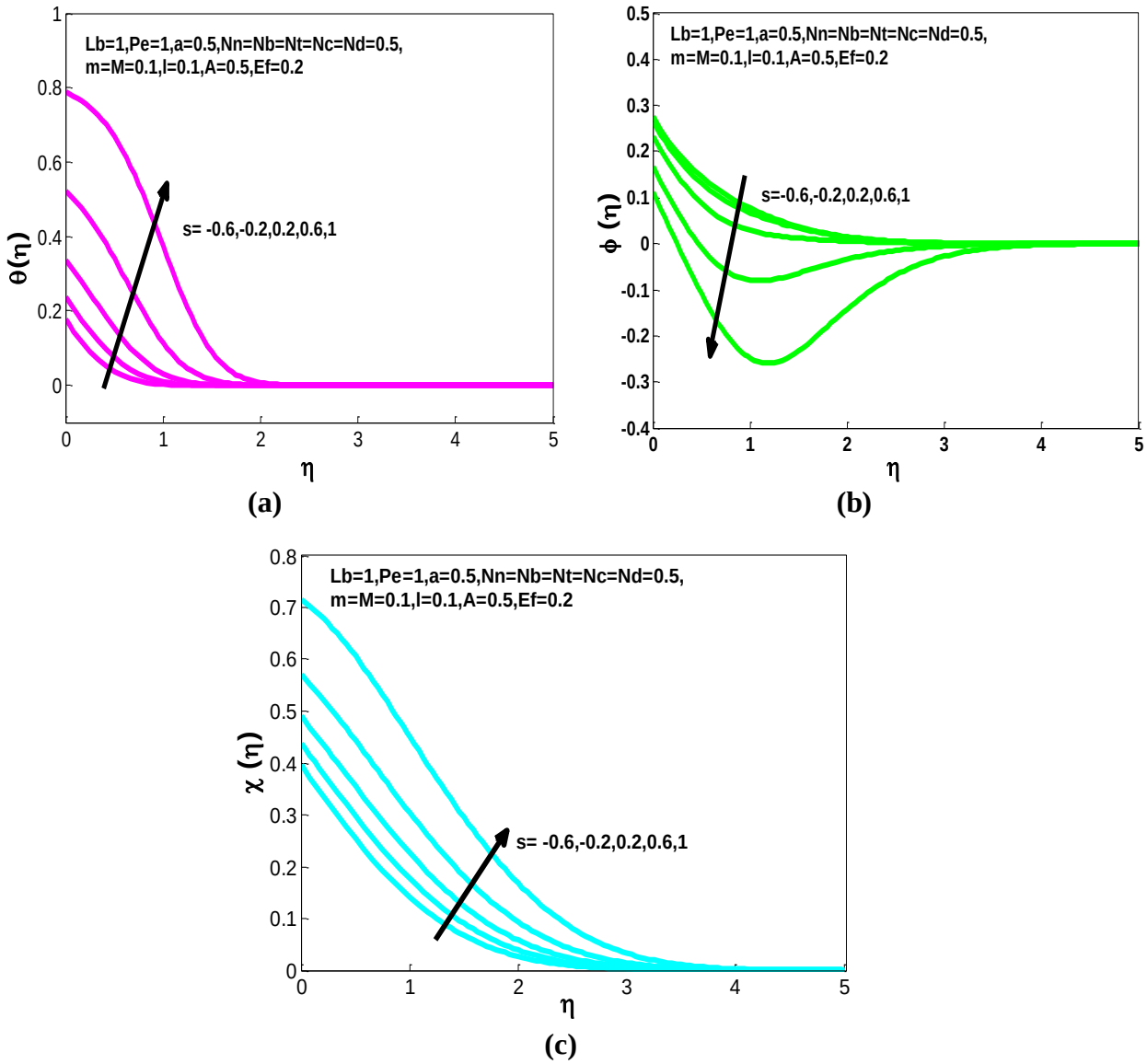

Fig.7: Effects of the blowing parameter ***s*** on the dimensionless (a) temperature (b) nanoparticle volume fraction and (c) micro-organismnumber density.

Thus, thermal boundary layer thickness is greater with mass injection into the boundary layer. A similar effect occurs in the motile micro-organism field. By blowing a greater quanitity of micro-organisms into the flow regime, this naturally results in greater concentration values. Conversely, the introduction of nanofluid reduces the concentration of nanoparticles since the scales involved amount to greater qunatities of base fluid comapred with nanoparticles. Suction reverses this process and intensifies the concentration distribution of nanoparticles.

5.7 Effects of the reciprocal of the magnetic Prandtl number, *A*

Figure 8 portrays the effects of the reciprocal of the magnetic Prandtl number $A = \frac{\xi}{\upsilon}$ on the fluid velocity and induced magnetic field with suction at the wall. This parameter is invoked due to magnetic induction effects and defines the ratio of magnetic diffusivity to viscous diffusivity. Magnetic Reynolds number is sufficiently large for the flow field to create magnetic field distortion. For cases where the value of this parameter is very small compared to unity, the magnetic field is known to be undistorted by the flow. However, for large values of magnetic Reynolds number, induction effects are significant and necessitate a separate conservation equation,as considered in the present model.As ***A*** increases, both the fluid velocity (**Fig.8(a)**) and induced magnetic field (**Fig.8(b)**) decrease. Momentum and magnetic boundary layer thicknesses will therebybe increased and decreased, respectively. It is also apparent that the effect of ***A*** is more pronounced on magnetic induction $h'(\eta)$ than $f'(\eta)$ at the wedge face.

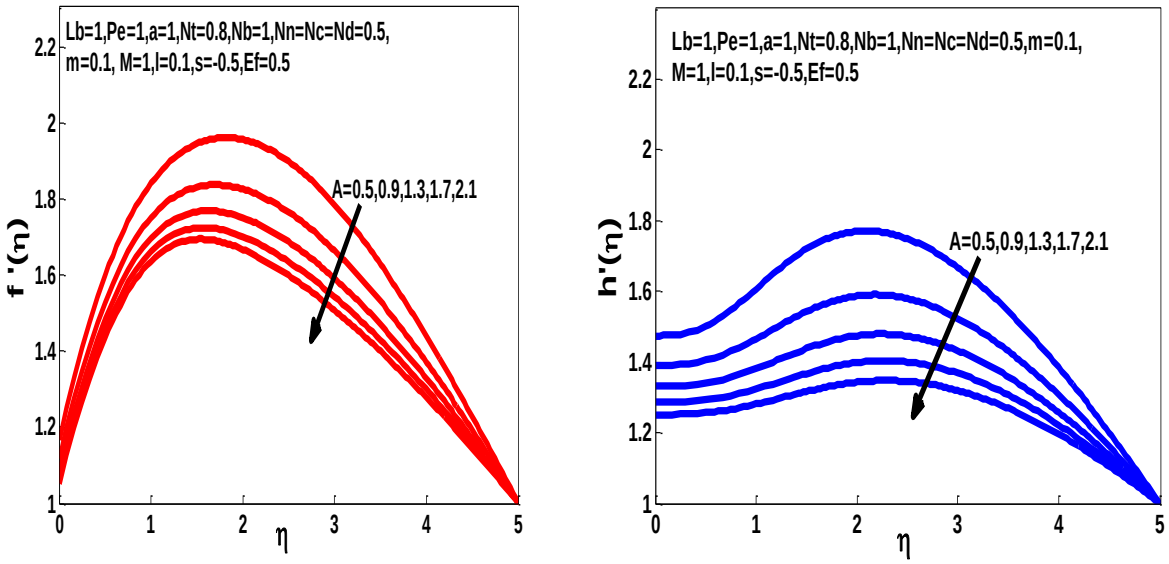

(a) (b)

Fig. 8: Effects of the reciprocal of the magnetic Prandtl number *A* on the dimensionless (a) velocity and (b) induced magnetic field.

5.8 Behaviour of Engineering Design Quantities

In **Fig.9(a)**,the skin frictioncoefficient $f''(0)$ is observed to rise with greater electric field parameter which is consistent with the earlier computation for velocity field (**Fig.3(a)**).A stronger aligned electric field accelerates the flow, generating greater shear at the wedge face. The primary effect of electric field E_f is to thin the hydrodynamic boundary layer, as opposed to transverse magnetic field M which induces deceleration and thickens the momentum boundary layer.Fluid dynamic control in conductive nanomaterials processing is thereby achievable via the imposition of both electric and magnetic fields. The suction effect $(s\langle 0)$ decreases surface shear stress i.e. skin friction and decelerates the boundary layer flow shearing past the wedge face. Blowing $(s\rangle 0)$ induces the opposite effect.

Figure 9(b) depicts the variation of the local Nusselt number $N_{u_{\bar{x}}}$, representing the heat transfer rate at the wedge surface, for different values of the wedge parameter (m) with respect to convection-conduction parameter (Nc) and Brownian motion parameter (Nb) for

very low wall injection ($s = 0.1$). The heat transfer rate increases with wedge parameter since the latter is associated with pressure gradient. This encourages heat removal from the boundary layer to the wall, as elucidated in [48]. Almost horizontal profiles are observed, indicating that the wedge parameter has a consistent and sustained influence on Nusselt number. A similar response has been determined by [49]. Nusselt number is also strongly enhanced with an increase in convection-conduction parameter. As computed previously,this decreases temperatures in the nanofluid and thusencouarges the migration of heat towards the wall (wedge face), boosting heat transfer to the wedge. Increased Brownian motion number (Nb) physically correlates with smaller nanoparticle diameters that cause greater temperatures in the nanofluid. Brownian motion encourages heat transfer away from the wedge face into the boundary layer, resulting in a slight depression in Nusselt number values. Therefore, smaller Brownian motion number corresponds to larger nanoparticles which achieve a reduced thermal enhancement. A boost in the temperature physically implies that heat diffuses faster in nanofluids than vortices. **Figure 9(c)**illustrates that the increase of thermophoresis Nt and diffusion-convection parameter Nd both enhance the local mass transfer rate for the flow near the wedge with suction present $(s = -0.1)$. Since thermophoresis is inversely proportional to thermal diffusivity and directly proportional to thermophoretic diffusion coefficient, mass transfer rate decreases with greater thermal diffusivity and increases with decreasing thermophoretic diffusion.Nanoparticle mass transfer rate at the wedge face is also found to be enhanced with increasing wedge parameter (m).

Figure 9d shows the effects of bio-convectionLewis number(Lb), micro-organism diffusion-convection parameter(Nn), and bio-convection Péclet number(Pe)on local micro-organism transfer rate. Péclet number is directly proportional to $\tilde{b}$ (chemotaxis constant) and Wc (maximum cell swimming speed) and inversely proportional to D_n (diffusivity of

microorganisms). Therefore, for higher Péclet number, the micro-organism speed will be reduced and/or the diffusivity of the micro-organisms will be decreased. This will result in reduced concentrations of micro-organism in the boundary layer and an elevation in motile micro-organism mass transfer rate as observed in **Fig.9(d)**. Micro-organism mass transfer rate also increases with the increase of bio-convection Lewis number and micro-organism diffusion-convection parameter. That is, with the increase of the thermal diffusivity the micro-organism mass transfer rate at the wedge face increases.

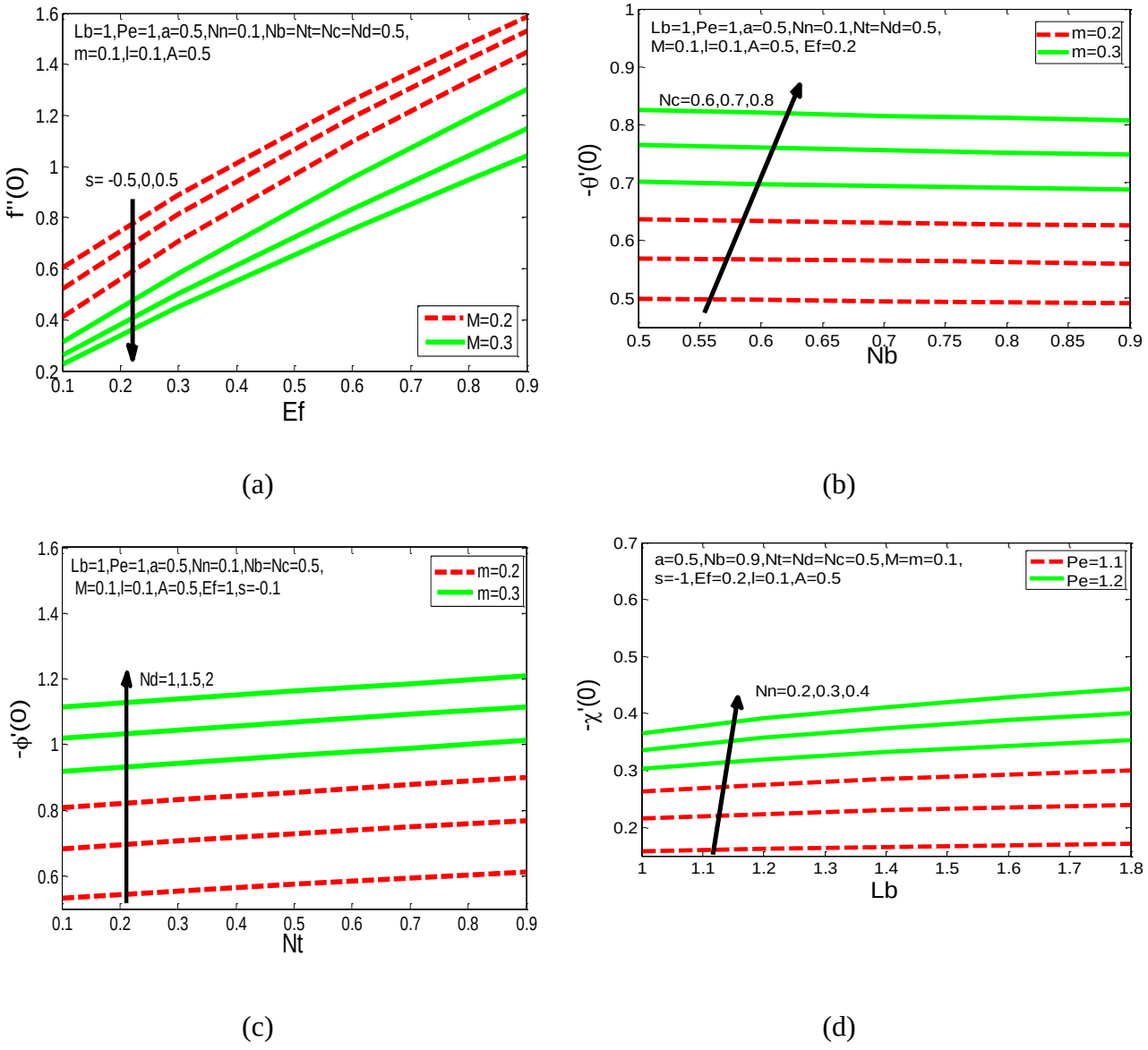

Fig.9: Results of (a)skin friction coefficient $C_{f\bar{x}}$, (b)local Nusselt number $Nu_{\bar{x}}$, (c)local Sherwood number $Sh_{\bar{x}}$, and (d) density number of motile micro-organisms $Nn_{\bar{x}}$ for varius

values of electric parameter, blowing parameter, magnetic field parameter, Brownian motion, convection-conduction parameter, wedge parameter, thermophoresis, diffusion-convection parameter, Lewis number, micro-organism diffusion-convection parameter and Péclet number, respectively.

6. CONCLUSIONS

A mathematical model has been developed for two-dimensional stagnation point flow, heat, mass and microorganism transfer along a wedge. The model incorporates the effects of both aligned (streamwise) electric field and transverse magnetic field, magnetic induction, multiple convective boundary conditions, hydrodynamic slip, and Stefan blowing. BVP5C finite difference numerical solutions have been obtained for the transformed, nonlinear boundary value problem. Selected computations have been presented and it has been shown that:

1. With an increase in magnetic field parameter, the temperature of the fluid decreases and nanoparticle volume fraction increases.
2. The temperature and micro-organism increases with the increase of electric field parameter whereas the nanoparticle volume fraction decreases.
3. The nanoparticle volume fraction decreases with an increase in the convection-conduction parameter.
4. With greater diffusion-convection parameter, the wedge flow is strongly decelerated whereas nanoparticle volume fraction is enhanced.
5. The micro-organism number density increases with micro-organism diffusion-convection parameter.
6. The skin friction parameter decreases with an increase in magnetic field parameter (due to stronger magnetohydrodynamic drag force) and blowing parameter whereas it is elevated with an increase in electric field parameter.

7. The heat transfer rate is reduced with greater Brownian motion parameter whereas it is boosted with increased convection-conduction and wedge parameters.
8. The local mass transfer rate increases with a rise in thermophoresis, diffusion-convection, and wedge parameters.
9. The local micro-organism transfer rate increases with higher bio-convection Lewis number, micro-organism diffusion-convection parameter and bio-convection Péclet number.
10. Magnetic induction (i.e. magnetic stream function gradient) is substantially enhanced with greater electric field parameter whereas it is reduced with increased values of the reciprocal of the magnetic Prandtl number.
11. Velocity is strongly decreased with increasing magnetic Prandtl number i.e. flow deceleration is induced.

The present investigation has addressed some novel features in bio-convection electromagnetic nanofluid transport from a wedge configuration using a *Newtonian* model. Future studies will consider *non-Newtonian* nanomaterials and will be communicated imminently.

Acknowledgement: The authors acknowledge financial support from Universiti Sains Malaysia, RU Grant 1001/PMATHS/811252. Authors also thankful to the reviewer for his/her valuable comments.

REFERENCES

[1] Castellanos. *Basic concepts and equations in electrohydrodynamics*, in: Springer Verlag, Wien, New York; 1998.

[2] Tripathi D**,** Bhushan S, Bég, O Anwar. Transverse magnetic field driven modification in unsteady peristaltic transport with electrical double layer effects, *Colloids Surfaces*

A Physicochem. Eng Asp 2016;506:32–39.

[3] Brouwer SP. *Design and characterization of a single effect EHD desalinator*. PhD Thesis, Delft University of Technology, Netherlands; 2011.

[4] Bég O Anwar, Hameed M, Bég TA. Chebyshev Spectral Collocation Simulation of Nonlinear Boundary Value Problems in Electrohydrodynamics. *Int J Comput Methods Eng Sci Mech* 2013;14:104–115.

[5] Tarantsev KV, Korosteleva AV. Optimization of design of ejector-type mixer for producing fuel emulsions in an electric field. *Chem Pet Eng* 2013;49:173–177.

[6] Pérez-Masiá R, López-Rubio A, Fabra MJ, Lagaron JM. Use of electrohydrodynamic processing to develop nanostructured materials for the preservation of the cold chain. *Innov. Food Sci Emerg Technol* 2014;26:415–423.

[7] Jang S, Kim Y, Oh JH. Influence of processing conditions and material properties on electrohydrodynamic direct patterning of a polymer solution. *J Electron Mate* 2016;45:2291–2298.

[8] Seyed-Yagoobi J. Electrohydrodynamic pumping of dielectric liquids. *J Electrostat.* 2005;63:861–869.

[9] Yabe A, Mori Y, Hijikata K. Active heat transfer enhancement by utilizing electric fields.*Annu. Rev. Heat Transf.*1996;7:193–244.

[10] Marucho M, Campo A. Electrohydrodynamic natural convection enhancement for horizontal axisymmetric bodies. *Int J Therm Sci* 2013;63:22–30.

[11] Atalik K, Sönmezler Ü. Symmetry groups and similarity analysis for boundary layer control over a wedge using electric forces. *Int J Non Linear. Mech* 2009;44:883–890.

[12] Atalık K, Sönmezler Ü. Heat transfer enhancement for boundary layer flow over a wedge by the use of electric fields. *Appl Math Model* 2011;35:4516–4525.

[13] Huang M, Lai FC. Numerical study of EHD-enhanced forced convection using two-

way coupling. *J Heat Transf* 2003;125:760.

[14] Vilela Mendes R, Dente JA. Boundary-layer control by electric fields. *ASME J. Fluids Eng* 1998;120:626.

[15] Furse C, Christensen DA, DurneyCH. *Basic introduction to bioelectromagnetics.*, CRC Press; 2009.

[16] Gaandhi OP (ed.).*Biological effects and medical applications of electromagnetic energy*, Englewood Cliffs, NJ (US);1990.

[17] Choi SUS, Eastman JA. Enhancing thermal conductivity of fluids with nanoparticles, *ASME Int.Mech Eng Congr Expo* 1995;66:99–105.

[18] Bég O Anwar, Uddin MJ, Khan, WA. BIoconvective non-newtonian nanofluid transport in porous media containing micro-organisms in a moving free stream. *J Mech Med Biol* 2015;15:1550071.

[19] Mody VV, Cox A, Shah S, Singh A, Bevins W, Parihar H. Magnetic nanoparticle drug delivery systems for targeting tumor. *Appl Nanosci* 2014;4:385–392.

[20] Beg O Anwar, Tripathi D. Mathematica simulation of peristaltic pumping with double-diffusive convection in nanofluids: a bio-nano-engineering model. *Proc Inst Mech Eng Part N J Nanoeng Nanosys* 2011;225:99–114.

[21] Rana P, Bhargava R, Bég O Anwar. Finite element modeling of conjugate mixed convection flow of Al_2O_3 –water nanofluid from an inclined slender hollow cylinder, *Phys. Scr.* 2013;87: 55005.

[22] Rana P, Bhargava R, Bég O Anwar, Kadir A. Finite Element Analysis of Viscoelastic Nanofluid Flow with Energy Dissipation and Internal Heat Source/Sink Effects. *Int J Appl Comput Math* 2016;1–27.

[23] Tripathi D, Bhushan S, Bég O Anwar, Akbar NS. Transient peristaltic diffusion of nanofluids: a model of micropumps in medical engineering, *J Hydrodyn. Ser B*, In

Press, 2016.

[24] Akbar NS, Shoaib M, Tripathi D, Bhushan S, Bég O Anwar. A study of entropy generation and heat transfer of CNT-nanofluids in flow driven by beating cilia through porous medium. *J Hydrodyn Ser B* ,In Press., 2016.

[25] Vékás L. Magnetic nanofluids properties and some applications. *Rom J Phys* .2004;49:707–721.

[26] Nkurikiyimfura I, Wang Y, Pan Z. Heat transfer enhancement by magnetic nanofluids—A review. *Renew Sustain Energy Rev* 2013;21:548–561.

[27] Shaw S, Sibanda P, Sutradhar A, Murthy PVSN. Magnetohydrodynamics and Soret effects on bioconvection in a porous medium saturated with a nanofluid containing gyrotactic microorganisms. *J Heat Transf* 2104;136:52601.

[28] Khan WA, Uddin MJ, Ismail AI. Bioconvective non-Newtonian nanofluid transport over a vertical plate in a porous medium containing microorganisms in a moving free stream. *J Porous Med* 2015;118:389–399.

[29] Mutuku WN, Makinde OD. Hydromagnetic bioconvection of nanofluid over a permeable vertical plate due to gyrotactic microorganisms. *Comput Fluids.*2014;5:88–97.

[30] Khan WA, Makinde OD. MHD nanofluid bioconvection due to gyrotactic microorganisms over a convectively heat stretching sheet. *Int J Therm Sci* 2014;81:118–124.

[31] Zaimi K, Ishak A, Pop I. Stagnation-point flow toward a stretching/shrinking sheet in a nanofluid containing both nanoparticles and gyrotactic microorganisms. *J Heat Transfer,2014;*136: 41705.

[32] Basir MF Md, Uddin MJ, Ismail AIMd, Bég O Anwar. Nanofluid slip flow over a stretching cylinder with Schmidt and Péclet number effects.*AIP Adv.*2016;6: 55316.

[33] Ali N, Asghar Z, Anwar Bég O, Sajid M. Bacterial gliding fluid dynamics on a layer of non-Newtonian slime: Perturbation and numerical study. *J Theor Biol* 2016;397:22–32.

[34] Sajid M, AliN, Bég O Anwar, Siddiqui AM. Swimming of a singly flagellated micro-organism in a magnetohydrodynamic second-order fluid. *J Mech Med Biol* 2016;1750009.

[35] Pérez-Masiá R, Fabra MJ, Chalco-Sandoval, W, López-Rubio A, Lagaron JM. Development by electrohydrodynamic processing of heat storage materials for multisectorial applications.*In: Springer International Publishing* 2015; 281–287.

[36] Zuo R. Biofilms: strategies for metal corrosion inhibition employing microorganisms. *Appl Microbiol Biotechnol* 2007;76:1245–53.

[37] Morikawa M. Beneficial biofilm formation by industrial bacteria Bacillus subtilis and related species. *J Biosci Bioeng* 2006;101:1–8.

[38] Rajagopal KR, Gupta AS, Na TY. A note on the Falkner-Skan flows of a non-newtonian fluid. *Int J Non Linear Mech* 1983;18:313–320.

[39] Davidson P A. *An Introduction to Magnetohydrodynamics*. Cambridge University Press, Cambridge; 2001.

[40] Blums E, Mikhailov Y, Ozols R.*Heat and Mass Transfer in MHD Flows*. World Scientific; 1987.

[41] Kuznetsov AV, Nield DA. Natural convective boundary-layer flow of a nanofluid past a vertical plate: A revised model. *Int. J. Therm. Sci.*2014;77:126–129.

[42] Dehghan M, Mahmoudi Y, Valipour MS, Saedodin S. Combined conduction–convection–radiation heat transfer of slip flow inside a micro-channel filled with a porous material. *Transp Porous Med* 2015;108:413–436.

[43] Abram S Dorfman.*Conjugate Problems in Convective Heat Transfer*. CRC Press;

2010.

[44] Hairer G, Lubich E, Wanner C. *Geometric Numerical Integration*.Second, Springer-Verlag, Berlin/Heidelberg; 2006.

[45] JafarK, Nazar R, Ishak A, Pop I. MHD boundary layer flow due to a moving wedge in a parallel stream with the induced magnetic field. *Bound Value Prob* 2016;20.

[46] Jaffe NA. Effects of a transverse magnetic field and spanwise electric field on the boundary layer of a conducting fluid. *A IAA J* 1966;4:1843–1846.

[47] Ibrahim FN, Terbeche M. Solutions of the laminar boundary layer equations for a conducting power law non-Newtonian fluid in a transverse magnetic field. *J Phys D Appl. Phys.*1994;27:740–747.

[48] *Laminar Boundary Layers.* Edited by L. Rosenhead. Oxford University Press; 1963.

[49] Zueco J, Bég O Anwar. Network simulation solutions for laminar radiating dissipative magneto-gas dynamic heat transfer over a wedge in non-Darcian porous regime. *Math Comput Model* 2009;50;439–452.